Materials Letters 403 (2026) 139507

Contents lists available at ScienceDirect

Materials Letters

journal homepage: www.elsevier.com/locate/matlet

Multiscale characterization of surface integrity of machined Inconel 718

Oliver Schenk [a,*], Mehrak Vahed Doost [a], Pascal Behrens genannt Wäcken [b], Markus Meurer [b], Thomas Bergs [b,c], Christoph Broeckmann [a]

[a] Institute for Materials Applications in Mechanical Engineering, RWTH Aachen University, Augustinerbach 4, Aachen, 52062, Germany
[b] Manufacturing Technology Institute MTI of RWTH Aachen University, Campus-Boulevard 30, Aachen, 52074, Germany
[c] Fraunhofer Institute for Production Technology (IPT), Steinbachstraße 17, Aachen, 52074, Germany

ARTICLE INFO

Keywords:
Surface integrity
TKD
Machining
White layer
Inconel 718

ABSTRACT

The surface integrity of Inconel 718 encompasses both the physical topography and the altered material properties beneath the surface, which depends on machining parameters such as depth of cut, feed and cutting speed. This study demonstrates the characterization of surface integrity by comparing different high-resolution methods. Passive force during turning was hereby identified as a key factor for subsurface deformation, whereas an increase of the thermomechanical load led to an increase in white layer, that was successfully investigated employing transmission-kikuchi-diffraction.

1. Introduction

The surface integrity after machining of materials such as Inconel 718 plays a critical role in service life, as imperfections introduced during finishing processes can act as initiation sites for fatigue cracks under operational stresses [1,2]. Widely investigated aspects of surface integrity of Inconel 718 encompass both the surface topography [3] and microstructural changes underneath the surface, such as white layer formation [2,4], work hardening [5–8] and the introduction of subsurface cracks [3]. In this respect, primary carbides being situated in subsurface regions are prone to fail due to complex shear stress states during turning.

To improve surface quality, extend service life and optimize the economic efficiency of production, a thorough understanding of the different aspects of surface integrity is essential [1,9], which requires appropriate experimental methods. Hence, this study presents various insights in surface integrity after turning of Inconel 718, utilizing scanning electron microscopy (SEM), transmission-kikuchi-diffraction (TKD), electron-back-scatter-diffraction (EBSD) and nanoindentation.

2. Experimental methods

In this work, Inconel 718 with a chemical composition given in Table 1 was investigated.

The material was solution annealed at 980 °C for 1 h, then air cooled. Rings with an inner diameter of 160 mm, an outer diameter of 171 mm and a thickness of 11.6 mm were machined afterwards. Aging was performed at 720 °C for 8 h in ambient atmosphere, followed by cooling to 620 °C at 50 °/h, a dwell time of 8 h and final air cooling.

The experiments were carried out on a NEF600 CNC lathe from DMG Mori without cutting fluid supply, since dry turning facilitates the derivation of cause–effect relationships and favours white layer formation [4]. The rings were internally clamped using a three-jaw chuck and machined by external longitudinal turning. Indexable inserts made of carbide blanks from Extramet (type EMT210) with a cobalt content of 10% (WC-Co10) were used, which were ground and subsequently PVD-coated with TiAlSiXN. Based on their macro-geometry, the inserts can be classified according to the ISO code CNMN120404. The ground and coated inserts are characterized by a sharp cutting edge radius of approximately 8.5 µm with a PVD coating thickness of 3–5 µm. A toolholder from Kennametal of type CCLNL2525M12-MN4 was used, resulting in an effective rake angle of −6° and a clearance angle of 6° in combination with the insert geometry. During machining, forces were measured using a three-component dynamometer of type 9129AA from Kistler. A single ring was turned with a cutting depth of 1.0 mm and a cutting speed of 30 m/min, whereas for a second ring, the cutting depth was decreased to 0.5 mm, while cutting speed was 60 m/min. The feed was constant with 0.15 mm/rev. Both parameter sets induced a material removal rate of 75 mm^3/s.

One cross section was extracted from each sample, embedded in electrically conductive resin, ground and polished. All investigations were carried out with a Helios Nanolab and a Tescan Clara SEM. EBSD measurements were conducted in the subsurface region enclosing an area of approximately 120 µm × 120 µm with a step size of 80 nm. The geometrically necessary dislocation (GND) density was computed with MTEX according to Pantleon [10], while excluding grain boundaries

* Corresponding author.
E-mail address: o.schenk@iwm.rwth-aachen.de (O. Schenk).

https://doi.org/10.1016/j.matlet.2025.139507
Received 24 July 2025; Received in revised form 1 September 2025; Accepted 12 September 2025
Available online 22 September 2025

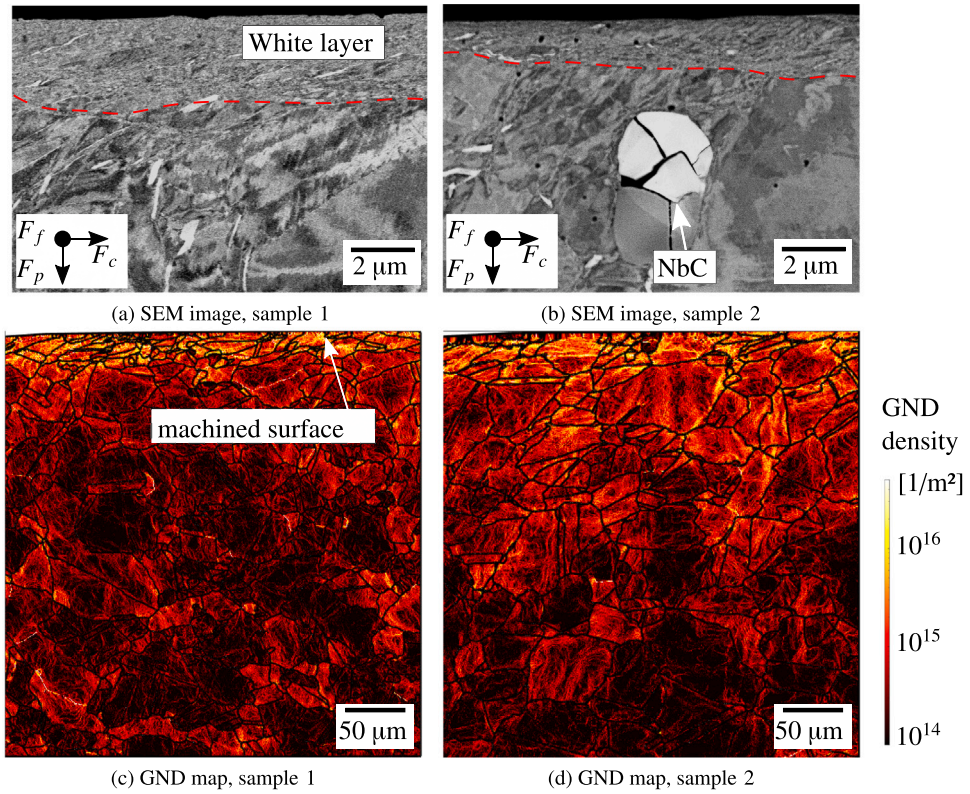

Fig. 1. SEM images and GND maps of the subsurface regions.

Table 1
Chemical composition in weight percent determined by optical emission spectroscopy.

Fe	Ni	Cr	Mo	Nb	Ti	Al	C	Mn	Si	Cu
Bal.	54.00	18.00	5.30	3.17	1.08	0.53	0.03	0.06	0.09	0.08

and their deformation. Furthermore, Young's moduli were calculated with respect to the force components in turning by incorporating the crystallographic orientations and orthotropic elasticity [11].

The thickness of the white layer was investigated by SEM, while TKD was used to quantify the grain size. The latter prerequired the preparation of a thin foil specimen that was extracted from the cutting surface utilizing a focused ion beam with 30 kV used for cutting and 5 kV for subsequent cleaning steps. Eventually, TKD measurement was performed with a step size of 7 nm.

One hardness profile was measured for each sample by nanoindentation using a Bruker Hysitron PI 89 SEM picoindenter with a Berkovich indenter. The indentation depth was 20 nm with a minimum distance between individual indents of 400 nm. The force was applied while imposing hysteresis loops that allow for the deduction of Young's modulus.

3. Results and discussion

The variation of cutting conditions induced significant changes in mechanical loads. Sample 1 was subjected to a cutting force F_c of 695 N, a passive force F_p of 227 N and a feed force F_f of 499 N. For sample 2, F_c and F_f decreased proportionally to 323 N and 200 N, which agrees qualitatively well to literature [12], while F_p remained rather constant at 196 N. The latter behaviour is both consistent with and contradictory to various publications [9,12,13].

While sample 1 exhibits a pronounced white layer with an averaged thickness of 2.69 µm, a thickness of approximately 1.05 µm was found for sample 2, as shown in Fig. 1(a) and (b). This may be attributed to the higher forces observed for sample 1 that may have induced a proportional heat generation. Additionally, fractured niobium carbides could be found in the vicinity of the surface of both samples, as depicted in Fig. 1(b).

Contrarily, GND density plots in Fig. 1(c) and (d) show a comparable degree of deformation underneath the white layer. This indicates that subsurface deformation is mainly affected by F_p, as the other force components would suggest a notable difference otherwise, agreeing with [9]. The areas close to the surface are rather homogeneously deformed, revealing high GND densities. Underneath, an inhomogeneous deformation with neighbouring grains exhibiting notable variations in GND density can be observed. However, the averaged GND depth-profiles, depicted in Fig. 2(a), reveal a similar decay in both samples, indicating comparable, average hardening of the subsurface region. Accordingly, similar grain sizes were found, with smaller grains being located close to the surface. This is in contrast to an expected increase in subsurface deformation and a decrease in grain size with an increase of cutting speed [5,8]. A comparable, opposing dependency was found for milling [6]. However, numerical investigation indicated a decrease of the depth of deformation with an increase of cutting speed [7]. These studies only considered the process parameters and not the cutting forces acting as the root cause.

Nanoindentation of both samples revealed an increase of hardness and young's modulus within the first few microns, with the latter corresponding to literature findings [2]. The obtained hardness, GND density and Young's modulus profiles are depicted in Fig. 2(c) to (f) along with the Young's modulus with respect to the direction of F_p being computed from EBSD measurement and then extracted along the measurement path from nanoindentation. The measured hardness profiles align well with the corresponding GND density profiles as both

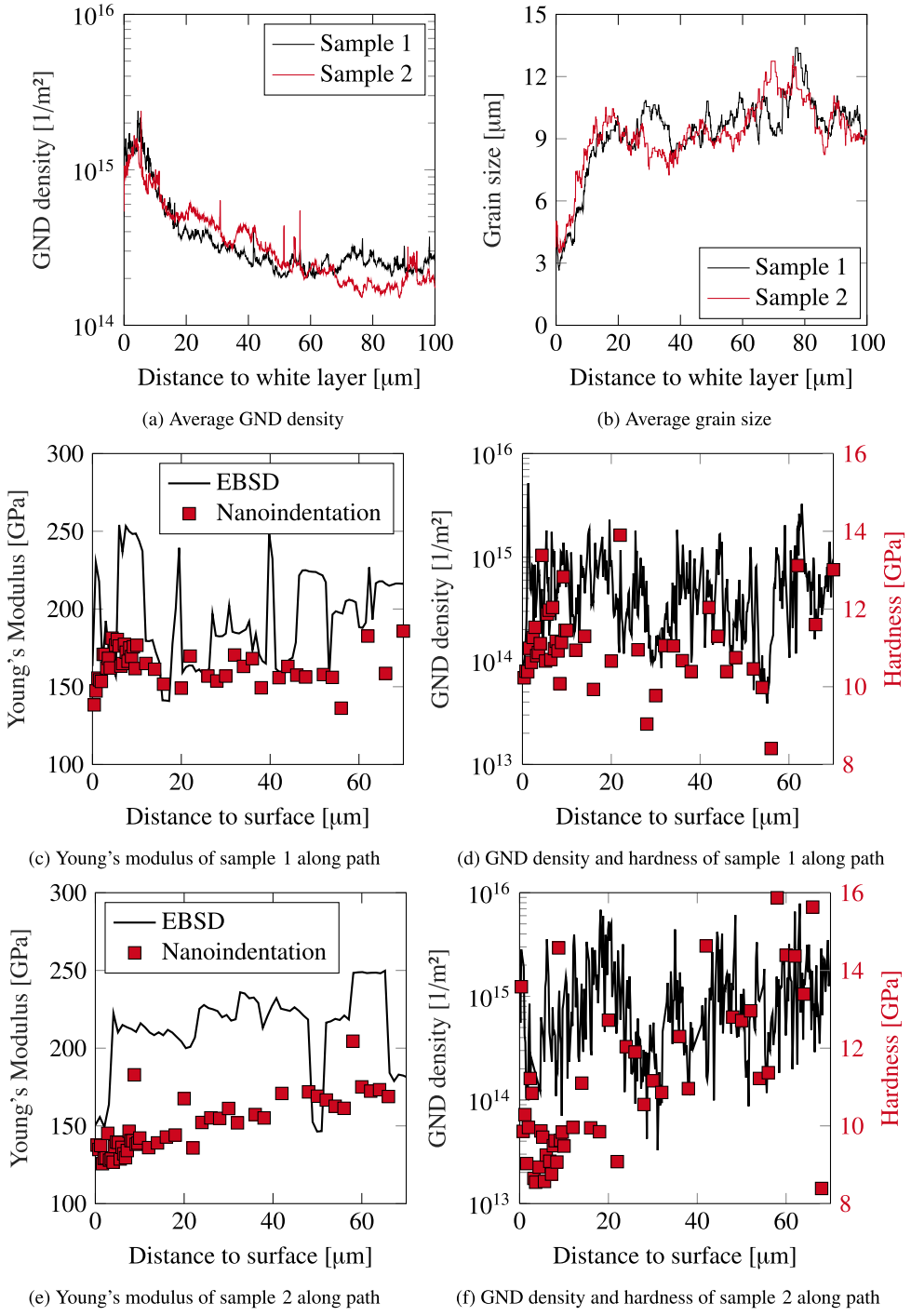

(a) Average GND density

(b) Average grain size

(c) Young's modulus of sample 1 along path

(d) GND density and hardness of sample 1 along path

(e) Young's modulus of sample 2 along path

(f) GND density and hardness of sample 2 along path

Fig. 2. Depth profiles of various microstructural and mechanical characteristics.

relate to work hardening. As dislocation density seem to correlate with the Young's modulus with respect to F_p, it may be postulated that the latter imposes a constant displacement, leading to higher stresses in grains with higher stiffness, while releaving other grains in their surrounding so that a preferable orientation of slip bands must not necessarily correlate with higher deformation of a grain.

The microstructure of the white layer is depicted as an inverse pole figure map with Fig. 3(a) showing the raw data, while Fig. 3(b) includes a subsequent reconstruction of grain boundaries and a smoothing using a halfquadratic filter. Average grain size increases exponentially from roughly 50 nm at the surface to 600 nm in the core, as indicated by Fig. 3(c). A comparable minimum grain size was deduced by applying Scherrer-equation to x-ray-diffraction measurements [1], whereas TKD measurements have exhibited insufficient indication to date [4].

4. Conclusions

SEM, EBSD, nanoindentation and TKD were employed to investigate surface integrity on Inconel 718 with each method contributing to a more holistic representation of the latter. A variation of cutting parameters induced significant changes in white layer thickness, while the extent of subsurface deformation remained unchanged. It was

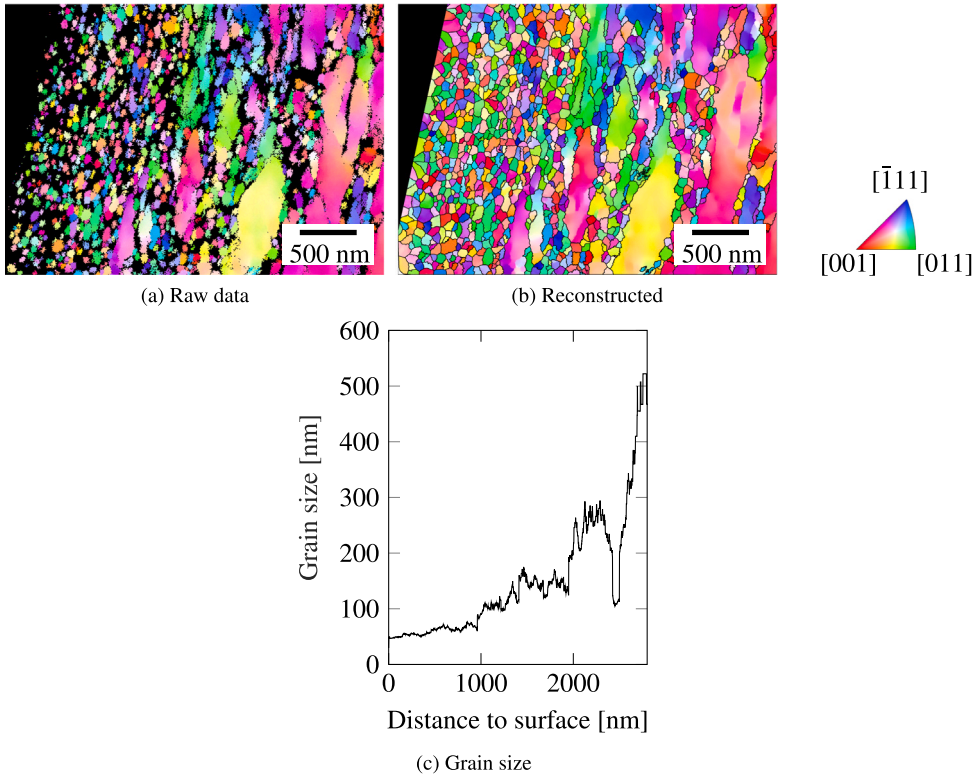

(a) Raw data (b) Reconstructed

(c) Grain size

Fig. 3. TKD measurement of white layer of sample 1.

concluded that the latter is mainly dependent on the passive force. On a mesoscale, heterogeneous deformation was observed which was attributed to the orientation of individual grains with grains with higher effective Young's modulus exhibit higher deformation. Hardness was found to correlate with GND density, so that nanoindentation can be considered supplementary to EBSD. TKD was successfully employed to quantify the grain size in the white layer, ranging from 50 to 600 nm.

CRediT authorship contribution statement

Oliver Schenk: Writing – review & editing, Writing – original draft, Visualization, Supervision, Methodology, Investigation, Data curation, Conceptualization. **Mehrak Vahed Doost:** Writing – original draft, Visualization, Investigation. **Pascal Behrens genannt Wäcken:** Writing – original draft, Investigation. **Markus Meurer:** Supervision. **Thomas Bergs:** Supervision, Funding acquisition. **Christoph Broeckmann:** Supervision, Funding acquisition.

Declaration of competing interest

The authors declare that they have no known competing financial interests or personal relationships that could have appeared to influence the work reported in this paper.

Acknowledgements

The authors appreciate the funding of this work by the Deutsche Forschungsgemeinschaft (DFG) – German Research Foundation for the project 494882739 "Experimental and model-based analysis of machining-induced residual stresses and part distortion when turning Inconel 718".

Data availability

Data will be made available on request.

References

[1] L.A.B. Marçal, H. Dierks, V. Bushlya, I. Lazar, D. Dzhigaev, Z. Ren, R. Rysov, A. Björling, M. Sprung, A. Mikkelsen, F. Lenrick, R. M'Saoubi, J. Wallentin, Spatially resolved structural and chemical properties of the white layer in machined Inconel 718 super alloy, Mater. Des. 239 (2024) 112789, http://dx.doi.org/10.1016/j.matdes.2024.112789.

[2] A.M. Wusatowska-Sarnek, B. Dubiel, A. Czyrska-Filemonowicz, P.R. Bhowal, N. Ben Salah, J.E. Klemberg-Sapieha, Microstructural characterization of the white etching layer in nickel-based superalloy, Met. Mater. Trans. A 42 (12) (2011) 3813–3825, http://dx.doi.org/10.1007/s11661-011-0779-8.

[3] A.R.C. Sharman, J.I. Hughes, K. Ridgway, Workpiece surface integrity and tool life issues when turning Inconel 718™ nickel based superalloy, Mach. Sci. Technol. 8 (3) (2004) 399–414, http://dx.doi.org/10.1081/MST-200039865.

[4] Z. Chen, M.H. Colliander, G. Sundell, R.L. Peng, J. Zhou, S. Johansson, J. Moverare, Nano-scale characterization of white layer in broached Inconel 718, Mater. Sci. Eng.: A 684 (2017) 373–384, http://dx.doi.org/10.1016/j.msea.2016.12.045.

[5] D. Xu, Z. Liao, D. Axinte, M. Hardy, A novel method to continuously map the surface integrity and cutting mechanism transition in various cutting conditions, Int. J. Mach. Tools Manuf. 151 (2020) 103529, http://dx.doi.org/10.1016/j.ijmachtools.2020.103529.

[6] H. Liu, M. Meurer, T. Bergs, Surface integrity analysis in orthogonal milling of Inconel 718, Procedia CIRP 123 (2024) 191–196, http://dx.doi.org/10.1016/j.procir.2024.05.035.

[7] S. Ranganath, C. Guo, P. Hegde, A finite element modeling approach to predicting white layer formation in nickel superalloys, CIRP Ann 58 (1) (2009) 77–80, http://dx.doi.org/10.1016/j.cirp.2009.03.109.

[8] Y. Qi, J. Zhang, M. Yi, C. Xu, P. Zhang, Z. Chen, G. Li, Study on the grain refinement mechanism of the machined surface of Inconel 718, J. Mater. Res. Technol. 29 (2024) 1729–1743, http://dx.doi.org/10.1016/j.jmrt.2024.01.202.

[9] A. Madariaga, J.A. Esnaola, E. Fernandez, P.J. Arrazola, A. Garay, F. Morel, Analysis of residual stress and work-hardened profiles on Inconel 718 when face turning with large-nose radius tools, Int. J. Adv. Manuf. Technol. 71 (9–12) (2014) 1587–1598, http://dx.doi.org/10.1007/s00170-013-5585-6.

[10] W. Pantleon, Resolving the geometrically necessary dislocation content by conventional electron backscattering diffraction, Scr. Mater. 58 (11) (2008) 994–997, http://dx.doi.org/10.1016/j.scriptamat.2008.01.050.
[11] C. Kumara, D. Deng, J. Moverare, P. Nylén, Modelling of anisotropic elastic properties in alloy 718 built by electron beam melting, Mater. Sci. Technol. 34 (5) (2018) 529–537, http://dx.doi.org/10.1080/02670836.2018.1426258.
[12] B. Toubhans, G. Fromentin, F. Viprey, H. Karaouni, T. Dorlin, Machinability of inconel 718 during turning: Cutting force model considering tool wear, influence on surface integrity, J. Mater. Process. Technol. 285 (2020) 116809, http://dx.doi.org/10.1016/j.jmatprotec.2020.116809.
[13] F. Matos, T. Silva, F. Marques, D. Figueiredo, P. Rosa, A. de Jesus, Machinability assessment of Inconel 718 turning using PCBN cutting tools, Procedia CIRP 117 (2023) 468–473, http://dx.doi.org/10.1016/j.procir.2023.03.079.